4 Interaction of sound with the seafloor

4.1 Reflection of sound at the seafloor

4.1.1 Fluid-fluid interface

We already considered the case of a plane wave incident on an interface between two media with differing acoustic impedance, see figure 1. Both media are assumed to be fluids with parameters (ρ_1, c_1) and (ρ_2, c_2). Medium 2 is called the reflecting medium.

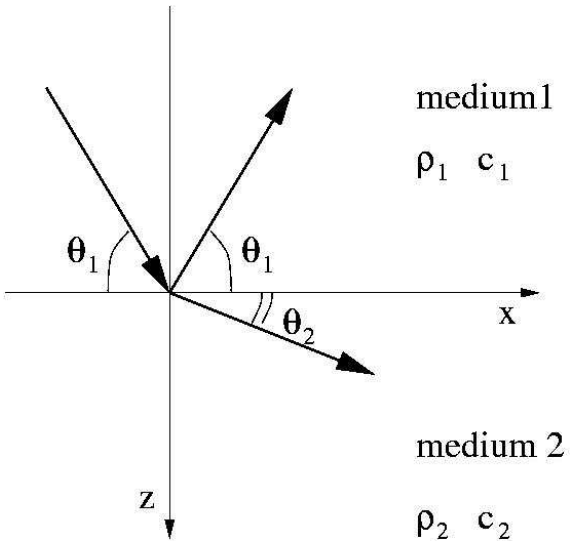

Figure 1

By applying the continuity conditions at the interface (for pressure and normal velocity) we have found Snell's law

$$\frac{\cos\theta_2}{c_2} = \frac{\cos\theta_1}{c_1} \tag{1}$$

and the expressions for the reflection and transmission coefficients:

$$R = \frac{\rho_2 c_2 \sin\theta_1 - \rho_1 c_1 \sin\theta_2}{\rho_2 c_2 \sin\theta_1 + \rho_1 c_1 \sin\theta_2} \tag{2}$$

$$T = 1 + R = \frac{2\rho_2 c_2 \sin\theta_1}{\rho_2 c_2 \sin\theta_1 + \rho_1 c_1 \sin\theta_2}. \tag{3}$$

If $c_2 > c_1$, there exists a critical given by

$$\theta_c = \arccos\left(\frac{c_1}{c_2}\right) \tag{4}$$

For $\theta_1 < \theta_c$ no compressional wave can propagate inside medium 2: R becomes complex with unit modulus independent of θ_1 ('total reflection'). When θ_1 increases while crossing the critical angle, R will suddenly decrease and then varies smoothly with θ_1. At normal incidence (θ_1 = 90°)

$$R = \frac{\rho_2 c_2 - \rho_1 c_1}{\rho_2 c_2 + \rho_1 c_1}. \tag{5}$$

Figures 2 and 3 show the modulus of R versus θ_1 where we varied c_2 and ρ_2 independently.

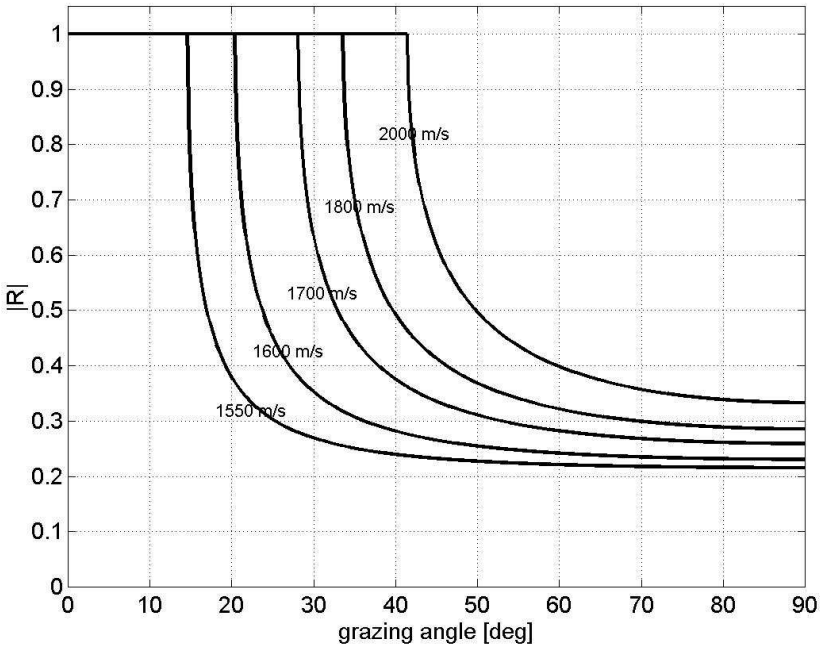

Figure 2: Parameter fixed: ρ_2 = 1.5.

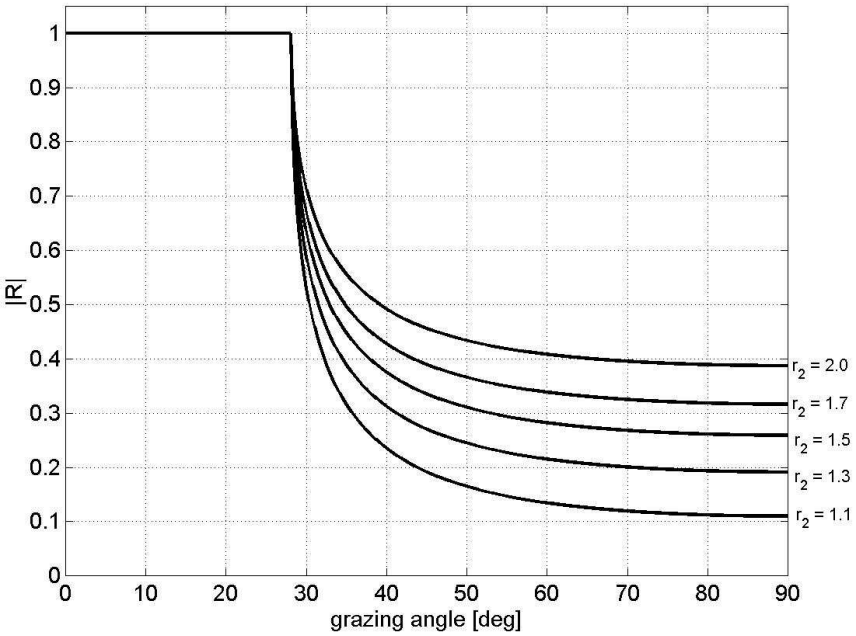

Figure 3: Parameter fixed: c_2 = 1700 m/s.

When $(\rho_2 c_2 > \rho_1 c_1, \quad c_2 < c_1)$ (i.e. for clayey bottoms) or when $(\rho_2 c_2 < \rho_1 c_1, \quad c_2 > c_1)$ (i.e. a non-physical situation) we have $R = 0$ at an angle θ_0, the angle of intromission, which is given by

$$\theta_0 = \arctan \sqrt{\frac{1-\left(\frac{c_2}{c_1}\right)^2}{\left(\frac{\rho_2 c_2}{\rho_1 c_1}\right)^2 - 1}} \qquad (6)$$

Equation (3) implies that the pressure of the transmitted wave may be higher than the pressure of the incident wave. This apparently surprising result only expresses continuity of pressure at the interface and does not violate conservation of energy. The plane wave intensity, projected on the vertical direction *z*, is conserved:

$$\frac{R^2}{2\rho_1 c_1}\sin\theta_1 + \frac{T^2}{2\rho_2 c_2}\sin\theta_2 = \frac{1}{2\rho_1 c_1}\sin\theta_1 \qquad (7)$$

4.1.2 Lossy reflecting medium

Absorption in the second medium is accounted for by making the wave number k_2, and hence the sound speed c_2, complex. Let α_2 be the absorption coefficient in medium 2

expressed in units of dB/λ (because often α_2 is considered to be proportional with frequency). The absorption coefficient in nepers/m is then given by

$$\alpha_2^{'} = \frac{\alpha_2}{\lambda_2 \, 20^{10} \log e} \qquad (8)$$

Here the factor $20^{10} \log e$ converts units nepers/m to dB/m, see section 3.1.9. $1/\lambda_2$ is the conversion from $1/\lambda$ to 1/m. $\alpha_2{}'$ is equal to the imaginary part of the wave number k_2 in the second medium:

$$k_2 \rightarrow k_2 + i\alpha_2^{'}$$

The imaginary part of the sound speed in the second medium then becomes:

$$\mathrm{Im}(c_2) \approx \frac{c_2 \alpha_2}{40\pi \, ^{10}\log e} \qquad (9)$$

The derivation for the reflection and transmission coefficients are still valid provided the complex expression for k_2 is used. The implication of absorption in the second medium is that an attenuated wave can always be transmitted and propagate through medium 2, even below the critical angle. Total reflection does not occur below the critical angle; $|R|$ is slightly below unity, see figure 4.

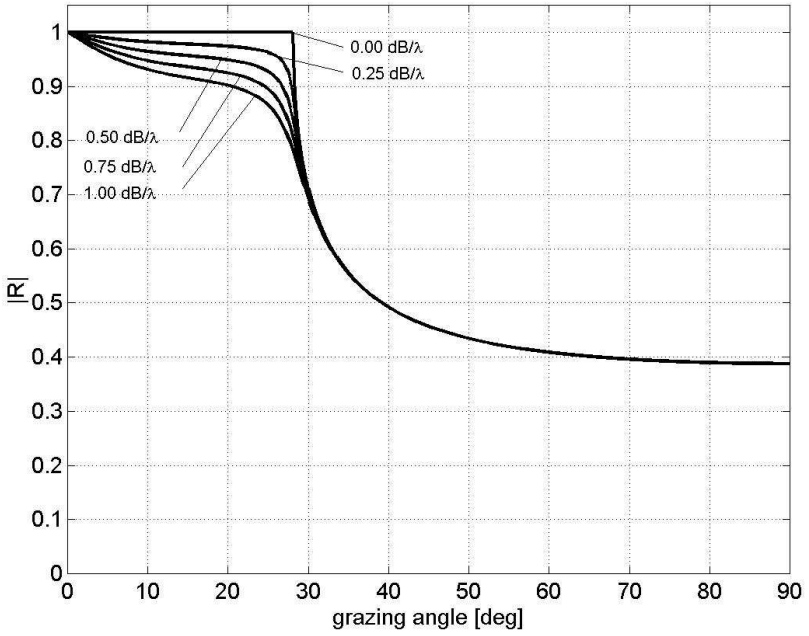

Figure 4: Parameters fixed: c_2 = 1700 m/s, ρ_2 = 2.

We will now consider the following unconsolidated sediments, the parameters of which are given table 1 below.

Table 1: geo-acoustic parameters of unconsolidated sediments.

Sediment type	M_z (ϕ)	n	ρ_2 g/cm^3]	c_2 [m/s]	α_2 [dB/λ]	$c_{s,2}$ [m/s]	h [cm]
Clay	9	0.80	1.2	1470	0.08	-	0.5
Silty clay	8	0.75	1.3	1485	0.10	-	0.5
Clayey silt	7	0.70	1.5	1515	0.15	125	0.6
Sand-silt-clay	6	0.65	1.6	1560	0.20	290	0.6
Sand-silt	5	0.60	1.7	1605	1.00	340	0.7
Silty sand	4	0.55	1.8	1650	1.10	390	0.7
Very fine sand	3	0.50	1.9	1680	1.00	410	1.0
Fine sand	2	0.45	1.95	1725	0.80	430	1.2
Coarse sand	1	0.40	2.0	1800	0.90	470	1.8

The mean grain size M_z in phi units is defined as

$$M_z[\phi] = -^2 \log(d[mm]) \qquad (10)$$

with d the average grain diameter in mm.
Density of the sediment is given by

$$\rho_2 = n\rho_1 + (1-n)\rho_b \qquad (11)$$

with n the porosity and ρ_b the bulk grain density (approx. 2.7 g/cm^3).
h is the standard deviation of the seafloor roughness amplitudes (see paragraph 3.4.2.2).

Figure 5 gives the reflection coefficient as a function of grazing angle for the 9 sediment types given in table 1 (shear is neglected).

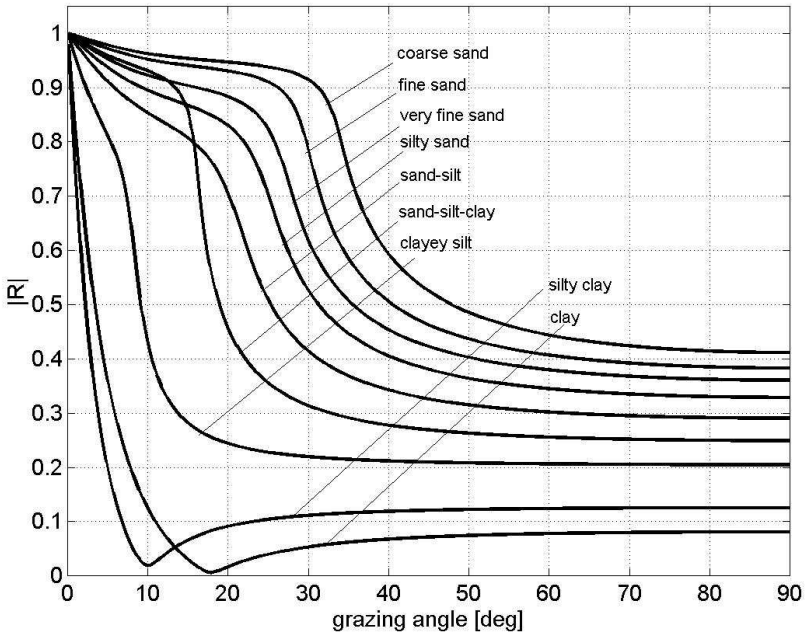

Figure 5

4.1.3 Elastic reflecting medium

When the second medium is solid and elastic, shear waves may propagate along with the compressional waves. The shear wave velocity $c_{s,2}$ is different from the sound velocity c_2 in such a way that

$$c_{s,2} < \frac{c_2}{\sqrt{2}} \tag{12}$$

The incident wave can potentially excite both the pressure wave and the shear wave. Snell's law now becomes

$$\frac{\cos\theta_1}{c_1} = \frac{\cos\theta_2}{c_2} = \frac{\cos\theta_{s,2}}{c_{s,2}} \tag{13}$$

The situation depends on the relative values of c_1, c_2 and $c_{2,s}$.
If $c_{s,2} < c_1$ the shear wave can always be excited, hence no total reflection can ever occur, even for $\theta < \theta_c$ (see figure 6a).

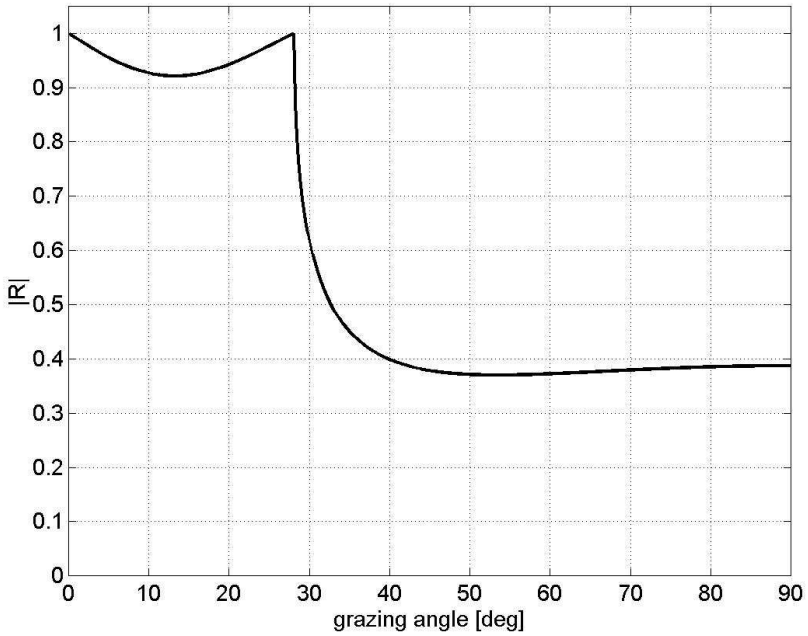

Figure 6a: c_2 = 1700 m/s, ρ_2 = 2, $c_{s,2}$ = 500 m/s, α_2 = 0.

If $c_{s,2} > c_1$, two critical angles exist:

$$\theta_c = \arccos\left(\frac{c_1}{c_2}\right)$$

$$\theta_{s,c} = \arccos\left(\frac{c_1}{c_{s,2}}\right) \qquad (14)$$

and there are three angular regimes now (see figure 6b):

- $\theta < \theta_{s,c}$: total reflection;
- $\theta_{s,c} < \theta < \theta_c$: only shear wave is transmitted;
- $\theta > \theta_c$: both pressure and shear wave is transmitted.

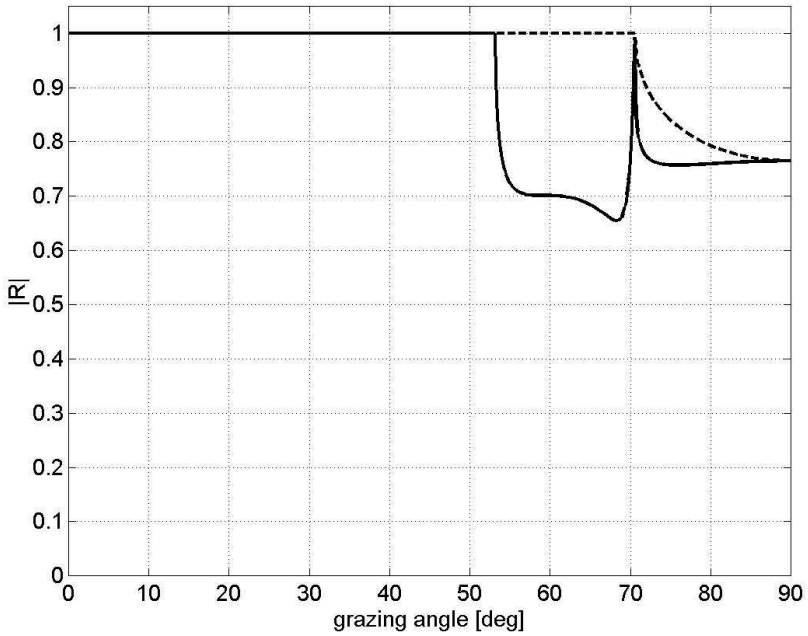

Figure 6b: c_2 = 4500 m/s, ρ_2 = 2.5, $c_{s,2}$ = 2500 m/s, α_2 = 0 (dashed line: $c_{s,2}$ = 0 m/s).

4.1.4 Layered reflecting medium

We now consider the three-layered fluid structure as depicted in figure 7. The reflection and transmission coefficients at the interface (i,j) are denoted $R_{i,j}$ and $T_{i,j}$.

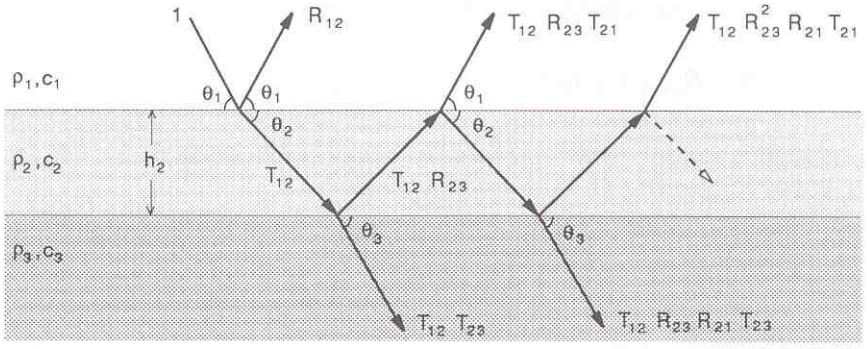

Figure 7

The total reflection coefficient can be written as

$$R = R_{12} + T_{12}R_{23}T_{21}\,e^{2i\varphi_2}\sum_{n=0}^{\infty}\left[R_{23}R_{21}\,e^{2i\varphi_2}\right]^n \qquad (15)$$

with

$$\varphi_2 = k_2 h_2 \sin\theta_2 \tag{16}$$

the vertical phase delay for a sound path crossing the layer of thickness h_2.
Using the sum for the infinite geometric series, we obtain

$$R = R_{12} + T_{12} R_{23} T_{21} e^{2i\varphi_2} \frac{1}{1 - R_{23} R_{21} e^{2i\varphi_2}} \tag{17}$$

We can further use

$$R_{21} = -R_{12} \tag{18}$$

and

$$T_{12} T_{21} = 1 - R_{12}^2 \tag{19}$$

thereby obtaining

$$R = \frac{R_{12} + R_{23} e^{2i\varphi_2}}{1 + R_{12} R_{23} e^{2i\varphi_2}} \tag{20}$$

The total reflection coefficient has become dependent on frequency. As before, the sound speeds can be complex to account for absorption in medium 2 and 3. Figure 8 presents an example. At low frequencies, medium 2 is practically transparent and *R* is similar to *R* of water (medium 1) – substratum (medium 3) interface. One can observe the critical angle associated with medium 3. As the frequency increases, resonance appears inside the layer due to multiple reflections between the boundaries. At the same time absorption inside the fluid layer becomes increasingly important, and the wave transmitted into the layer progressively becomes unable to reach the substratum. Finally, *R* is given by the contrast at the upper boundary.

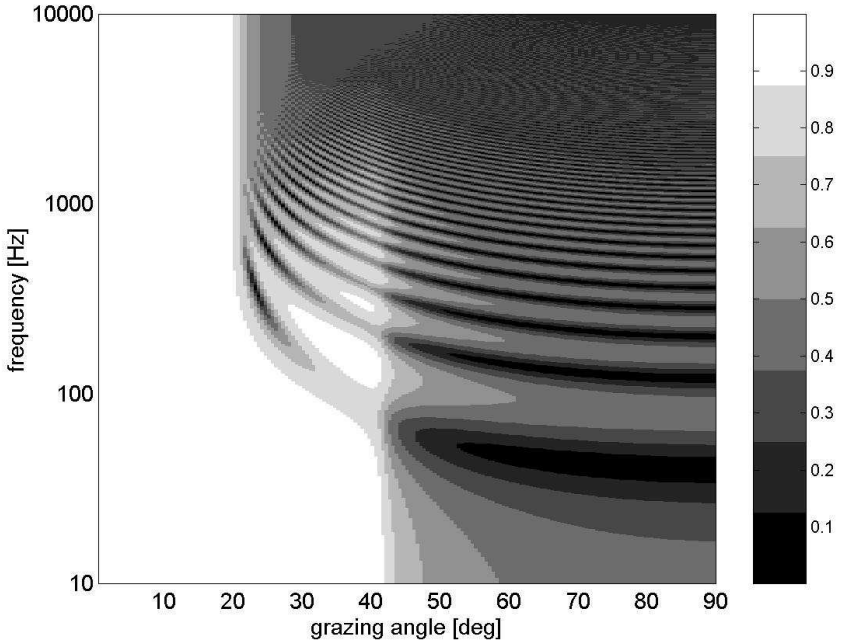

Figure 8: Parameters: c_2 = 1600 m/s, ρ_2 = 1.5, α_2 = 0.2 dB/λ, h_2 = 10 m, c_3 = 2000 m/s, ρ_3 = 1.5, α_3 = 0.5 dB/λ.

4.2 Scattering of sound at the seafloor

4.2.1 The physics of scattering

The seafloor is usually far from an ideal plane surface. The acoustic processes will therefore be much more complex than described above. The water-seafloor interface may be considered as locally plane, on average, with a microscale roughness whose influence will be significant if its characteristic dimensions are at least comparable with the acoustic wavelength. The effect of relief on the incident acoustic wave will depend on the frequency, the angle of incidence and the local characteristics of the relief. Interface irregularities will scatter the incident wave in all directions. Part of the incident wave will be reflected with no deformation other than an amplitude loss in the specular direction (the so-called coherent part). The remainder of the energy is scattered in the entire space, including back towards the source (the backscattered part). This process is depicted in figure 9 below.

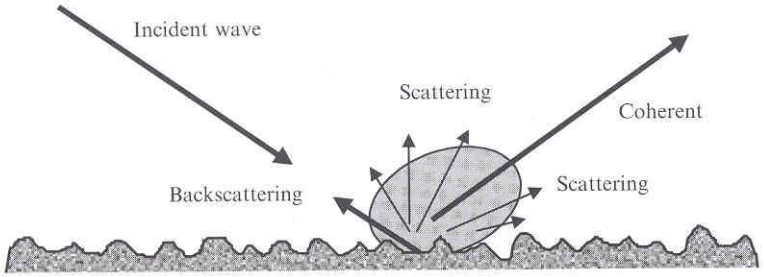

Figure 9

The relative importance of the specular and scattered components will depend on surface roughness in terms of the acoustic wavelength. Surfaces which appear rough to short acoustic wavelengths will appear smooth to long acoustic wavelengths.
Low interface roughness will induce a relatively larger specular component and low scattering distributed around the specular direction. On the other hand, high interface roughness will strongly attenuate the specular component and spread the scattering in all directions. Typical directional patterns for different conditions of seafloor roughness and impedance contrast are given in figure 10.

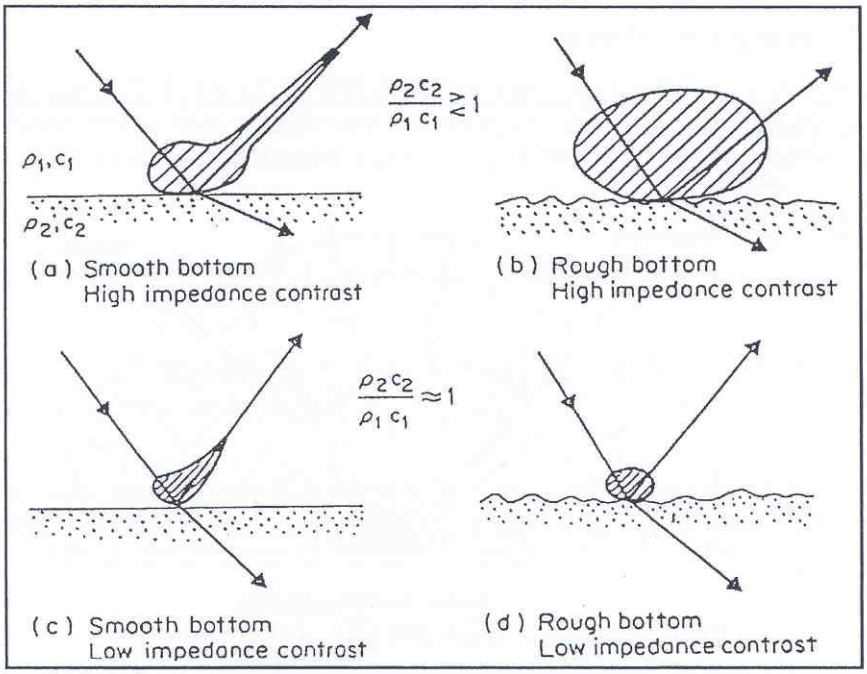

Figure 10

4.2.2 The spatial roughness spectrum

Microscale roughness on the seafloor has various possible origins and presents a wide scale of amplitudes ranging between a millimetre and a few meters. Several micro-

roughness scales coexist on the same surface. For instance, on a sandy seafloor, the sand waves have a centimetre-scale roughness, superimposed on the existing topography. In this case, the two roughness scales might correspond to different physical processes, depending on their size relative to the acoustic wavelength.
We will therefore introduce the concept of the spatial spectrum of the relief to quantify the amplitude distribution of a rough surface. It shows the energy distribution of the different harmonic components of the relief and is obtained by Fourier transforming the relief. Every spatial spectrum component is defined by a wave number $\kappa = 2\pi / \Lambda$, Λ being the spatial wavelength, see figure 11.

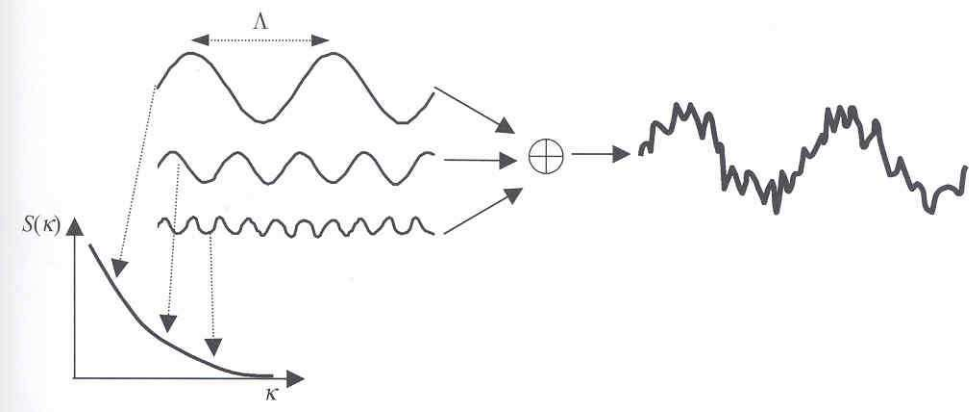

Figure 11

The spectrum can have specific, strong components if the relief is periodic (e.g. regular sand ripples). It can also be continuous if the relief is completely random. In the latter case one often uses a spectrum of the type

$$S(\kappa) = S_0 \, \kappa^{-\gamma} \qquad (21)$$

with γ approximately equal to 3.
In principle, the spatial spectrum should be considered along one particular direction. However, in practice, the relief is often assumed to be isotropic, with a spectrum independent of direction. (This assumption is obviously not valid in the case of the sand ripples).
The expression for the spatial spectrum, equation (18) is normalised according to

$$\int S(\kappa) \, d\kappa = h^2 \qquad (22)$$

with *h* the standard deviation of the relief amplitudes. Guideline values for *h* are given in table 1.

4.2.3 Reflection revisited – the Rayleigh parameter

Interface roughness can be quantified by the Rayleigh parameter:

$$P = 2kh\sin\theta \qquad (23)$$

with $k = 2\pi/\lambda$ the acoustic wave number, h the standard deviation of the relief amplitudes and θ the grazing angle of incidence. The coherent or specular component of the reflected wave can be described by

$$R_c(\theta) = R(\theta)e^{-P^2/2} = R(\theta)e^{-2k^2h^2\sin^2\theta} \qquad (24)$$

with R the reflection coefficient for the interface without relief. This 'model' is valid when P is small: $P < \pi/2$. For larger values of P the coherently reflected wave becomes negligible and the scattered field is dominant.
Figure 12 illustrates the effect of interface roughness for a coarse sand sediment (see table 1 for the parameters) for various frequencies. At 20 kHz the 'Rayleigh parameter model' is not valid at all angles (as indicated by the dashed line in the figure).

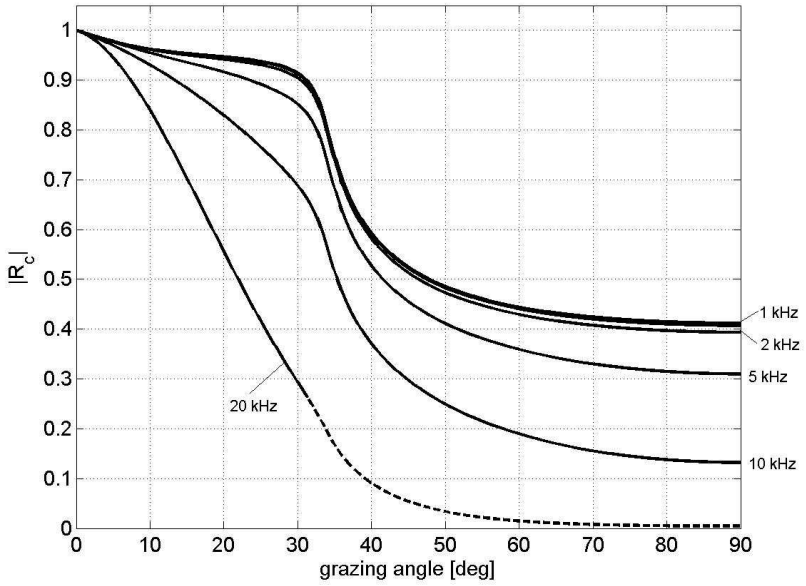

Figure 12

4.2.4 The scattering strength

The fundamental scattering quantity is the so-called backscattering strength defined as

$$S = 10^{10} \log \frac{I_s}{I_i} \qquad (25)$$

i.e. the ratio in dB's of the intensity I_s of the scattered sound from a unit area of 1 m^2 at a distance of 1 m from this unit area, and the intensity I_i of the incoming plane wave (see figure 13). We refer to 'backscattering' for the scattered sound in the direction of the source (indicated by point P in the figure).

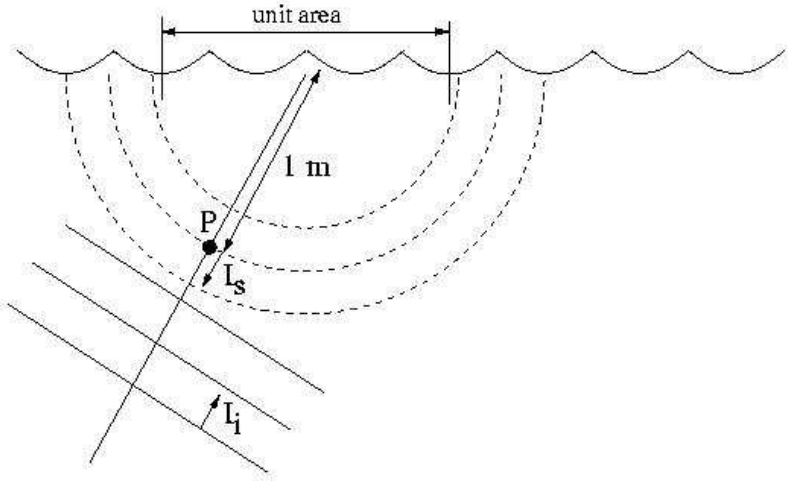

Figure 13

The scattering strength *S* of the seafloor potentially depends on seafloor type (roughness), frequency *f* and the grazing angle of incidence θ. In general, scattering strength increases with increasing θ. Frequency dependence and seafloor type dependence is much more complicated. For some types of seafloor *S* increases with increasing *f*, while other seafloor types exhibit hardly any frequency dependence (e.g. when the scale of roughness is large compared to the acoustic wavelength).
Apart from seafloor roughness, also inhomogeneities in the bottom can contribute to the scattering of sound and hence the scattering strength.

4.2.5 Lambert's rule

A frequently used formula for the backscattering strength is the so-called 'Lambert rule'. This rule provides a specific θ-dependence according to which many rough surfaces behave. It is not only applied in acoustics, but also in optics.
We consider the situation as depicted in figure 14.

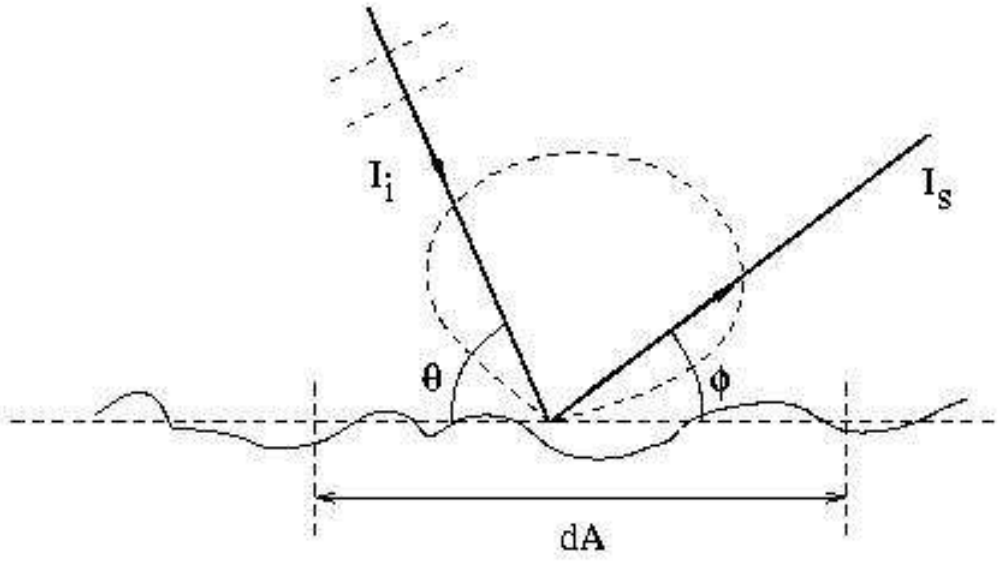

Figure 14

I_i is the intensity of a plane wave impinging on a rough seafloor at a grazing angle of incidence θ. The power intercepted by the bottom surface dA is equal to $I_i \sin\theta \, dA$. This power is assumed, by Lambert's rule, to be scattered proportional to the sine of the angle of scattering φ. The intensity I_s in the direction φ at a distance of 1 m from dA is then given by:

$$I_s = \mu(I_i \sin\theta \, dA)\sin\varphi \qquad (26)$$

where μ is a proportionality constant. For a unit area dA of 1 m^2 we can write

$$10^{10}\log\frac{I_s}{I_i} = 10^{10}\log\mu + 10^{10}\log(\sin\theta \sin\varphi)$$

The backscattering strength, for which $\varphi = 180° - \theta$, then becomes

$$S = 10^{10}\log\mu + 10^{10}\log(\sin^2\theta) \qquad (27)$$

In principle, the frequency and seafloor type dependence can be put in the parameter μ. Practically observed values of $10^{10}\log\mu$ range between –40 dB and –10 dB. At high frequencies there is evidence that $10^{10}\log\mu$ increases with grain size. A useful starting value for $10^{10}\log\mu$ for all types of seafloor is –27 dB. Figure 15 presents S as function of θ for this value of μ.

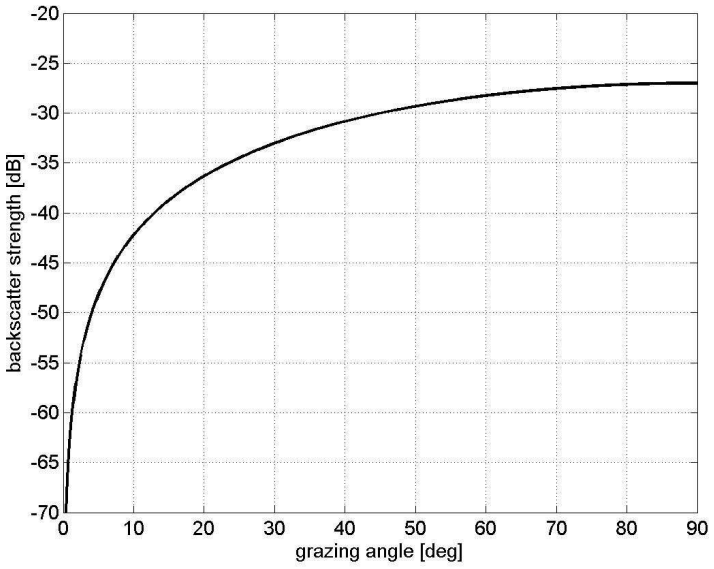

Figure 15

If all the incident acoustic energy is redistributed into the upper medium, with none lost by transmission into the medium below, it can be shown that $\mu_{\max} = 1/\pi$ (i.e. $10\ ^{10}\log \mu_{\max} = -5$ dB).

4.2.6 More sophisticated scattering strength models

Figure 16 gives modelled backscattering strength as a function of incidence angle (90°-θ) for the 9 different seafloor types given in table 2 and for a frequency of 100 kHz. These results were obtained assuming scattering is due to facet scattering near vertical incidence combined with Bragg scattering and volume scattering due to inhomogeneities (buried stones, shells, crustaceans, gas bubbles) in the sediment volume. The three different components are plotted as thin lines, whereas the total backscattering strength is plotted as a thick line. From clay to clayey silt, volume scattering dominates at grazing angles, whereas from sand-silt to coarse sand, Bragg scattering dominates.

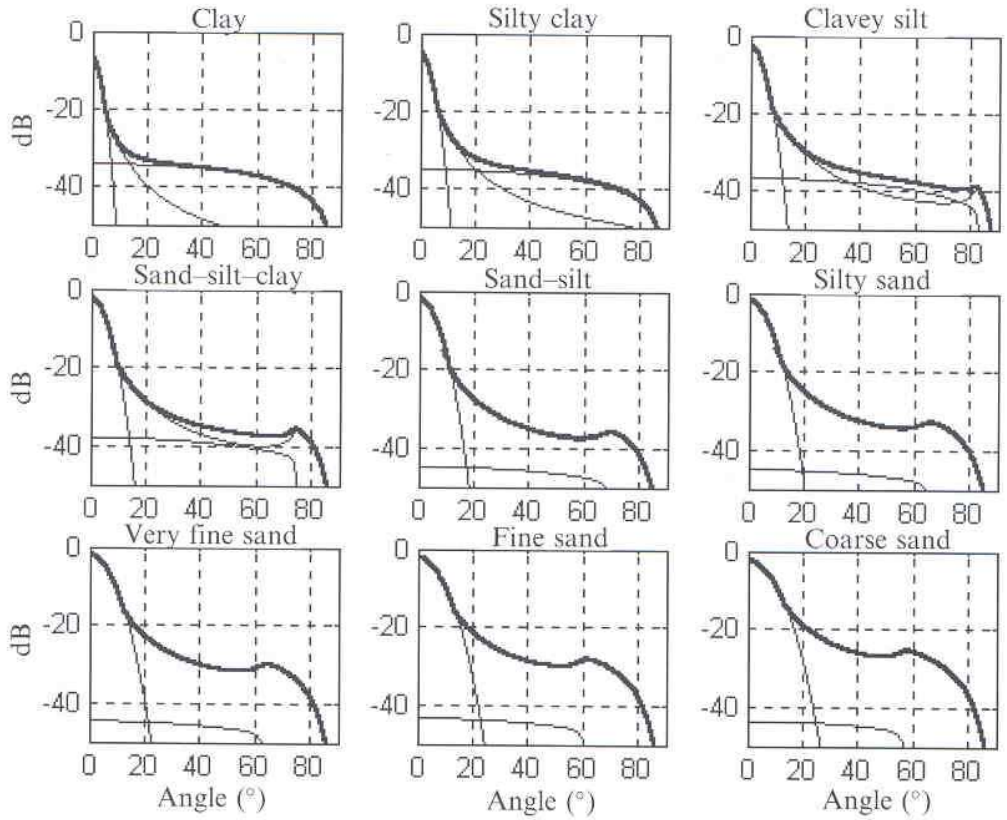
Clay
Silty clay
Clavey silt
Sand–silt–clay
Sand–silt
Silty sand
Very fine sand
Fine sand
Coarse sand
dB
0
-20
-40
0 20 40 60 80
Angle (°)

Figure 16